

## Aeration Due to Breaking Waves. Part II: Fluxes

A. GRAHAM\*

*School of Ocean and Earth Science, Southampton Oceanography Centre, University of Southampton, Southampton, United Kingdom*

(Manuscript received 6 December 2001, in final form 25 August 2003)

### ABSTRACT

Measurements have recently been obtained of bubble concentrations at a coastal shelf-sea site. A simple model of the generation of persistent bubble clouds by wind waves as they break, and of the subsequent evolution of the clouds, is here developed that harnesses these measurements. Estimates are derived of the frequency of wave breaking, the volume of air entrained on cessation of breaking, and the rate of transfer of carbon dioxide between bubbles and water in the clouds. Bubble clouds are generated at an estimated rate,  $50\chi^2(g/\lambda^5)^{1/2}$ , per unit sea surface area, where  $\chi$  is the dominant wave slope, or ratio of significant wave height  $H_s$  to energetically dominant wavelength  $\lambda$ , and  $g$  is the acceleration due to gravity. Cloud generation contributes a term,  $500\chi^4$ , to the active whitecap fraction. Entrainment distributes bubbles over a volume of equivalent hemispherical radius,  $2H_s$ . The large-scale turbulence surviving breaking is insufficient to sustain bubbles—by opposing their buoyancy—to the largest size held stable while rising by surface tension. The bubble size distribution on cessation of breaking is instead predicted to fall off rapidly for bubbles in excess of a radius,  $a_m = 7 \times 10^{-3}(\nu^2\lambda^3/g)^{1/6}$ , where  $\nu$  is the kinematic viscosity of seawater. At a (10 m) wind speed of  $10 \text{ m s}^{-1}$  at the site, the volume of air entrained per unit area of sea surface—the upward displacement of the surface by bubbles—is estimated to be a factor of 3 times  $a_m$  on cessation of breaking. The transfer of carbon dioxide following breaking within the clouds is insignificant.

### 1. Introduction

An acoustic study of bubble concentrations has been made as part of a recent experiment to investigate air–sea exchanges, as described in a companion paper (Graham et al. 2004; hereinafter Part I). Here, related fluxes are estimated. The difficulty in directly measuring breaking wave parameters forces the use of a model. The one developed here simulates the evolution of bubble clouds generated when wind waves break in deep water (Thorpe 1986; Osborn et al. 1992). Its free parameters are set using the acoustic measurements. It must apply from the cessation of breaking to a time of some 20 wave periods afterward, when measurements on the clouds are typically obtained. Extrapolating over this time period can clearly yield zero-order estimates only; this constitutes the principal limiting uncertainty.

Waves break and entrain air at sea in dispersive interactions between and within wave groups (see the re-

view section of Part I). Breaking is thus longitudinally and laterally localized. It takes place over a wide range of wavelengths,  $O(1 \text{ cm}–100 \text{ m})$  (Melville 1996) and may even exhibit fractal characteristics (Kerman and Bernier 1994; Belcher and Vassilicos 1997). Air is entrained during breaking—as is evident through whitecapping—for breaking wavelengths of order 1 m or more (the flow at such scales then being fully turbulent). At somewhat larger scales persistent bubble clouds form, lasting one to two orders of magnitude longer than the breaking. The variability between clouds modeled is that arising through their differing ages.

There is variability and structure in the bubble distribution within clouds. Some of this may arise through the presence of a roller vortex generated during breaking and of a rotor vortex thereafter (Thorpe 1995). A smaller rotor generated in secondary splash may also be of significance (Rapp and Melville 1990; Lamarre and Melville 1994; Thorpe 1995). Persistent streamwise vortices may be generated that replace the fluid swept away in the roller (Gemrich and Hasse 1992; Csanady 1994; Nepf et al. 1995). Boils may also be generated in the wake of bubbles returning to the surface (Thorpe et al. 1999). It would, however, be inappropriate to seek representation of such processes within the model. It is sought simply to model the evolving scales of the region of entrained air and of the bubbles in which, following breaking, air can be said to reside in a fairly stable manner.

\* Current affiliation: Department of Environmental and Geographical Sciences, Manchester Metropolitan University, Manchester, United Kingdom.

*Corresponding author address:* Dr. A. Graham, Dept. of Environmental and Geographical Sciences, Manchester Metropolitan University, John Dalton Building, Chester St., Manchester M1 5GD, United Kingdom.  
E-mail: a.graham@mmu.ac.uk

Bubbles can be taken, then, to be dispersed within a turbulent patch of water generated during breaking (see also Osborn et al. 1992). They persist below the surface as a result of downward motions within the patch that oppose their buoyancy, motions that continue to draw bubbles downward long after breaking (Dahl and Jessup 1995). The strongest downward motions may thus be assumed to be of paramount importance in governing the residence time of the bubbles, after which bubbles tend to reach the surface and burst.

The turbulent patch may be taken to scale with its largest eddies. These eddies may, in turn, be taken to have the largest convective velocity scales. The eddies will interact with the water's surface, as turbulence is inhibited there and a flattening of eddies takes place (Hunt and Graham 1978). They will couple with coherent structures within the patch, some of which may carry a bubbly signature, as described above. They will also interact with turbulent components of the mixed layer about them of comparable scale, particularly eddies generated in previous breaking events, and any large-scale Langmuir circulations.

Whether these interactions should, however, be considered controlling in the evolution of the patch is another matter. Eddies of comparable scale generated in previous breaking events will be less energetic, and any coupling thus likely weak. Langmuir circulation may strongly influence the character of turbulence in the vicinity of its downwelling zones, but many wave periods may be expected to elapse before the patch is entrained into a zone. This is probably why the circulation appears to affect characteristic bubble concentrations only weakly (see the conclusion of Part I). It is the earlier period when the turbulence is strong and much of the air entrained on cessation of breaking remains subsurface that is the more important, and that is of interest here.

The presence of the surface likely constitutes a more active dynamical constraint. Weight should also be given to the coherent structures within the patch or, more generally, the anisotropies of forcing with which they are associated. A spanwise vorticity increasing toward the patch's center is likely to emerge from wave breaking, and a vertical vorticity that increases toward its edges. Against these effects, however, must be counted the readiness with which the theory of homogeneous, isotropic, decaying turbulence can be extended beyond the equilibrium subrange in many different situations with transient and three-dimensional forcing to predict leading characteristics of the largest eddies (Batchelor 1953). This approximation explains much of the theory's enduring usefulness. It is, in consequence, invoked here: the anisotropies are taken not to be foremost in the evolution of the largest eddies and are not incorporated within the model.

The size of a bubble within a turbulent patch changes over its lifetime, as it exchanges oxygen and nitrogen with its surroundings and as its depth and corresponding hydrostatic pressure change (Thorpe 1982; Woolf and

Thorpe 1991). The enhanced pressure causes bubbles to lose gas, forcing surface waters to a supersaturated state. Surface tension in a bubble raises the pressure above hydrostatic values, but by 10% or more only for bubbles of less than about 10- $\mu\text{m}$  radius, so the hydrostatic effect is the dominant one. Most of the bubbles and the bubble-summed surface area and volume arise, however, within a significant wave height of the sea surface. A bubble of 50- $\mu\text{m}$  radius will scavenge a coating of surface-active material and persist at a depth of 1.5 m in saturated conditions for about 3 min (see Thorpe 1982). The effect of dissolution is weaker on shorter time scales and for larger bubbles, and is secondary in relation to present uncertainties in the form of the initial bubble size distribution. The effect, and any bubble amalgamation occurring once a population of stable bubbles has formed, are therefore not represented, and fractional changes in bubble volume are ignored.

With the viscous drag on a bubble and its buoyancy in balance, it rises at a steady speed with respect to the surrounding water, depending on its size and coating (Harper 1972; Thorpe 1982).

## 2. Model

Free parameters of the model are deduced in this section.

Bubble clouds at sea are taken to reside within a turbulent patch generated when waves break. Eddies within the patch are ascribed a dependence on an effective time since their inception. There are significant anisotropies associated with the generated patch, but it is postulated that these need not be invoked to account for the manner in which eddies evolve following breaking, even at the largest scales (see section 1). The largest eddies may thus be ascribed single length and convective-velocity scales  $L$  and  $V$ , respectively, and the patch be taken to occupy a hemisphere of radius equal to  $L$ , as shown in Fig. 1; see also Table 1. It also follows that characteristics of the breaking process cannot contribute to the dimensions of  $L$  and  $V$  and that these must therefore follow from a time since inception and the kinematic viscosity of water,  $\nu$  ( $1.3 \times 10^{-6} \text{ m}^2 \text{ s}^{-1}$ ), alone.

Breaking and bubble-cloud generation are represented in the model only simply as concomitant events instantaneously giving rise to a turbulent patch of bubbly water. The scales of the patch and largest eddies at generation are those following were the patch generated at a point a time,  $\Delta t$ , beforehand. It is to be expected that  $\Delta t$ , on evaluation, will compare to the duration of breaking obtaining in reality. A wave that breaks and entrains air does so over a length in the wave direction of around 0.5 wavelength (see the review section of Part I), from which it can be seen that breaking lasts for about 0.5 wave period.

The scales of the largest eddies a time  $\tau$  after breaking are thus taken as the following:

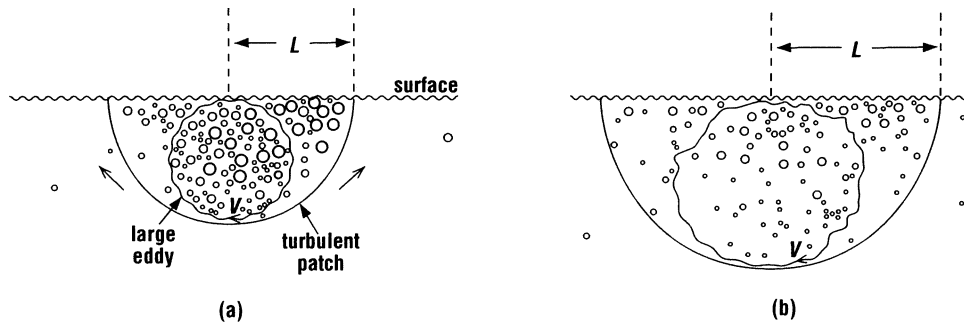


FIG. 1. Schematic of a bubble cloud as represented in the model (a) on cessation of breaking and (b) some time afterward. Symbols are as in the text.

$$L = Q_L[\nu(\Delta t + \tau)]^{1/2} \quad \text{and} \quad (1)$$

$$V = Q_V[\nu/(\Delta t + \tau)]^{1/2}, \quad (2)$$

where the coefficients,  $Q_L$  and  $Q_V$ , may depend on dimensionless wave parameters.

If  $\tau \gg \Delta t$ , the growth rate of the patch, the differential of (1) with respect to  $\tau$ , scales as patch age to the power  $-0.5$ . At sea, Dahl and Jessup (1995) observed bubble clouds to deepen at a rate settling to scale as cloud age to the power  $-0.3$ . In the laboratory, Rapp and Melville

TABLE 1. Nomenclature.

$a$	bubble radius
$a_m$	limiting $a$
$A_b$	total bubble surface area under unit sea surface
$B$	$\pi\nu(Q_L\Delta t)^2N/2$
$C_a$ ( $C_w$ )	bulk concentrations of trace gas in air (water)
$D_r$	characteristic residence depth of bubble clouds
$f_b$	frequency of bubble-cloud generation at a point at the surface
$f_i$	frequency at which new clouds are detected in an Eulerian frame at depth $D_r$
$g$	acceleration due to gravity
$G$	normalized bubble-radius size density
$H_s$	significant wave height
$k_L, k_N, k_v, k_\lambda$	constant dimensionless coefficients
$K_b$	trace-gas-transfer velocity associated with a population of bubbles
$L$	length scale of the largest eddies resulting from breaking
$m_b$	mass of trace gas in a bubble
$\dot{m}_b$	rate of change of $m_b$
$M$	power of $\chi$ in $N$
$N$	frequency of bubble-cloud generation per unit sea surface area
$p$	density of $P$
$P$	probability of observing a bubble cloud at the surface
$q$	power of $a$ in $G$
$Q_a, Q_L, Q_V$	dimensionless coefficients
$Re_b$	bubble Reynolds number
$t_b$	duration of breaking
$T$	dominant wave period
$v$	current speed
$v_b$	bubble rise speed
$V$	convective-velocity scale of the largest eddies resulting from breaking
$W_{10}$	wind speed at 10 m
$z_b$	upward displacement of the sea surface by bubbles
$\beta$	solubility coefficient of trace gas
$\gamma$	wave age
$\Delta m_b$	offset of $m_b$ from its equilibrium value
$\Delta t$	bubble-cloud-generation timescale
$\kappa_b$	trace-gas-transfer velocity associated with a single bubble
$\Lambda$	wavelength
$\lambda$	dominant $\Lambda$
$\nu$	kinematic viscosity of seawater
$\tau, \tau_t$	times since breaking
$\tau_*$	$\tau/\Delta t$
$\tau_c$	time constant of adjustment to equilibrium of trace gas in a bubble
$\chi$	wave slope $H_s/\lambda$

(1990) observed the turbulent patch generated by breaking planar waves to deepen at a rate settling to scale as patch age to the power  $-0.75$ , the planar form responsible for the faster falloff (Lamarre and Melville, 1994; see also the review section of Part I).

Bubbles in the turbulent patch rise with respect to the surrounding water at a steady speed,  $v_b$ . The dependence of  $v_b$  on bubble radius  $a$  is described by Harper (1972). Bubbles experience a drag of coefficient scaling with the inverse of the bubble Froude number,  $v_b^2/(2ga)$ , where  $g$  is the acceleration due to gravity ( $9.8 \text{ m s}^{-2}$ ). For small bubbles, the coefficient separately scales with the inverse of the bubble Reynolds number,  $\text{Re}_b \doteq 2av_b/\nu$ . Larger bubbles, which contribute most to the total bubble surface area and volume, exhibit higher coefficients than would follow from an  $\text{Re}_b^{-1}$  scaling. The flow stagnates behind bubbles of radius  $100 \mu\text{m}$  or more, corresponding to  $\text{Re}_b \geq 1$ . Bubbles of more than about  $500\text{-}\mu\text{m}$  radius, corresponding to  $\text{Re}_b \geq 200$ , experience a dynamic pressure difference as they rise that may exceed their excess pressure due to surface tension (the bubble Weber number thus exceeding unity). Sphericity is thus lost and bubble stability declines.

A drag coefficient scaling with  $\text{Re}_b^{-1/2}$  is deemed, for current purposes, to hold for the bubbles surviving wave breaking. It follows that

$$v_b = Q_a(g^2/\nu)^{1/3}a, \quad (3)$$

where  $Q_a$  is a constant coefficient assigned a value of  $0.57$ . A bubble of  $100\text{-}\mu\text{m}$  radius thus rises, from (3), at  $2.4 \text{ cm s}^{-1}$ .

A form must be ascribed, pragmatically and with a minimum of free parameters, to the size distribution of bubbles in the turbulent patch. Bubbles at *all depths* contribute to the distribution. While it is not possible from current understanding to account adequately for the origin or location of the distribution peak, it is clear that the falloff with radius becomes steep—as to a power more negative than  $-5$ —within a wave period of bubble generation (Deane and Stokes 2002). The falloff is thus supposed steep for bubbles in excess of a radius  $a_m$  at which  $v_b = V$  (see section 1). Bubbles are taken to remain subsurface while  $v_b < V$  and thereafter to return instantaneously to the surface, with the distribution peaking at  $a_m$ . The increase of the distribution with radius is as determined at the cessation of breaking (with gas dissolution being ignored, as discussed in section 1) and is that of a monomial of some degree,  $q$ , to be established. It may be anticipated that, if the distribution is narrow and the peak radius in reality is close to  $a_m$ , a value of  $q > 1$  will best map the model distribution to the true form. Conversely, if the distribution in reality reaches peak or near-peak values for bubbles significantly smaller than  $a_m$ , a value of  $q < 1$  should prove appropriate. Prescription of a more likely distribution form is described in Part I. The hypothesis that losses to the surface limit bubble size from the cessation of breaking onward is tested in the following section.

Radius  $a_m(\tau)$  follows on equating (2) and (3):

$$a_m/a_m(0) = (1 + \tau_*)^{-1/2}, \quad (4)$$

where

$$a_m(0) = (Q_v/Q_a)(\nu^5/g^4)^{1/6}/\Delta t^{1/2}, \quad (5)$$

and  $\tau_* \doteq \tau/\Delta t$ . The normalized size density,  $G(a, \tau)$ , is given by

$$G = \begin{cases} (q+1)(a/a_m)^q/a_m, & a \leq a_m \\ 0, & a > a_m. \end{cases} \quad (6)$$

The flux of a liquid-phase-limited trace gas supported by bubbles is now considered, the approach similar to that of Woolf (1993). The bubbles may be taken to be in a thermodynamic steady state (see section 1). The mass of trace gas in a bubble,  $m_b(\tau)$ , tends to an equilibrium value,  $m_b(\infty)$ , at a rate,  $\dot{m}_b$ , proportional to the offset from equilibrium,  $\Delta m_b \doteq m_b - m_b(\infty)$ . Offset  $\Delta m_b$  consequently falls (in magnitude) exponentially with time, the time constant  $\tau_c$  satisfying  $\tau_c = -\Delta m_b(0)/\Delta \dot{m}_b(0) = -\Delta m_b(0)/\dot{m}_b(0)$ . Offset  $\Delta m_b(0)$  is related to the bulk gas concentrations in air and water,  $C_a$  and  $C_w$ , respectively, according to  $\Delta m_b(0) = (4/3)\pi a^3(C_a - C_w/\beta)$ , where  $\beta$  is the equilibrium ratio of concentrations in water and air following from Henry's law. The rate of transfer to the water from the bubble,  $-\dot{m}_b(0)$ , may, furthermore, be related to the offset of gas concentration from equilibrium and the area over which exchange takes place. The relation is analogous to that adopted for fluxes across the sea surface (see the introduction to Part I): through the agency of a single-bubble transfer velocity,  $\kappa_b$ , it follows that  $\dot{m}_b(0) = -4\pi a^2\kappa_b(\beta C_a - C_w)$ . Substituting these expressions into that for  $\tau_c$ , it follows that  $\tau_c = a/(3\beta\kappa_b)$ . Because  $\dot{m}_b = \Delta \dot{m}_b = -\Delta m_b(0) \exp\{-\tau/\tau_c\}/\tau_c$ , further substitution of expressions for  $\Delta m_b(0)$  and  $\tau_c$  leads to a relation:

$$\dot{m}_b = -4\pi a^2\kappa_b \exp(-3\beta\kappa_b\tau/a)(\beta C_a - C_w). \quad (7)$$

Laboratory experiments indicate that, unless the water is highly pure, the rise speed and transfer velocity of a bubble less than  $500\text{-}\mu\text{m}$  radius are those of a rigid particle (Clift et al. 1978). The bubble quickly acquires a coating of impurities that sets up a tangential stress at its surface and inhibits internal circulation. The dependence of  $\kappa_b$  on bubble size is then weak and may to first order be neglected.

The bubble population that develops at sea is taken to result from an ensemble of turbulent bubbly patches generated independently of one another. Waves in deep water may break successively within a common group as they advance to the center where wave heights are greatest (Donelan et al. 1972; Thorpe and Hall 1983; Smith et al. 1996), but this association is not deemed strong enough to require representation within the model. The existence of any diffuse bubble layer below the patches, forming as the generation of each new patch disrupts older ones, is similarly neglected.

An expression for the probability of a turbulent bubble patch of age  $\tau_i$  or younger being present at an observation point at the surface,  $P(\tau \leq \tau_i)$ , is now sought. Whether the observation is made at a random instant in an Eulerian frame or a random location in a Lagrangian frame is immaterial, so the latter frame is adopted for ease of derivation. Let the mean rate at which patches are generated per unit sea surface area be denoted  $N$ . It can be seen that, in a time interval  $d\tau$ , the probability of observing a new patch,  $dP(d\tau)$ , is that of the patch's generation within a certain distance of the observation point, equal to the radius of the patch currently there. Thus, from (1),  $dP(d\tau) = \pi Q_L^2 \nu (\Delta t + \tau_i) N d\tau$ . As generation events occur independently, it follows that

$$1 - P(\tau \leq \tau_i + d\tau) = [1 - P(\tau \leq \tau_i)][1 - dP(d\tau)], \quad (8)$$

which may be expanded to yield

$$\begin{aligned} P(\tau \leq \tau_i + d\tau) - P(\tau \leq \tau_i) \\ = [1 - P(\tau \leq \tau_i)]dP(d\tau). \end{aligned} \quad (9)$$

Substituting for  $dP$  and rearranging it follows that

$$\begin{aligned} [P(\tau \leq \tau_i + d\tau) - P(\tau \leq \tau_i)]/d\tau \\ = \pi Q_L^2 \nu (\Delta t + \tau_i) N [1 - P(\tau \leq \tau_i)]. \end{aligned} \quad (10)$$

The limiting value of the left-hand side is the probability density, and the associated differential equation has as its solution,

$$P(\tau \leq \tau_i) = 1 - \exp[-\pi Q_L^2 \nu (\Delta t + \tau_i/2) N \tau_i]. \quad (11)$$

Differentiating this and normalizing to obtain the density,  $p(\tau_*)$ , gives

$$p(\tau_*) = 2B(1 + \tau_*) \exp[-B(2 + \tau_*)\tau_*], \quad (12)$$

where

$$B \doteq \pi \nu (Q_L \Delta t)^2 N / 2. \quad (13)$$

These relations are used in following appendices to calculate parameters of bubble populations and gas exchange that may be compared with the measurements (Part I).

### 3. Estimates

#### a. Bubble-cloud distribution

The dependence of model parameters on conditions is now addressed.

Sonar images of bubble clouds have been obtained at sea and used to assess the frequency with which clouds occur in an Eulerian reference frame (see section 4b of Part I). Clouds are identified objectively from the images using a technique that captures the large-scale strongly scattering coherent structure present. The measured mean frequency shows a subsurface maximum,  $f_i$ , at a depth referred to as that of characteristic cloud

residence  $D_r$  (as is evident, e.g., in Fig. 3 of Part I). Depth  $D_r$  may broadly be taken to scale as 2 times the significant wave height  $H_s$ , although the evidence suggests it is not directly determined by the dominant waves (see section 5a of Part I).

Depth  $D_r$  is interpreted in the context of the model as that to which bubble clouds characteristically penetrate when generated. Above this, some clouds are not identified as a result of inhomogeneities arising during breaking. Below this, bubble concentrations fall off as clouds evolve following breaking and acoustic back-scattering levels that approach those of noise. Assuming that at cessation of breaking bubbles are distributed throughout the turbulent patch engendered, the identification,  $Q_L(\nu \Delta t)^{1/2} = D_r$ , may then be made from (1) (with  $\tau = 0$ ).

The scale of breaking in the direction of the waves, expressed as a fraction of the dominant wavelength  $\lambda$ , may be calculated. In the model, the turbulent patch extends on generation over a scale at the surface equal to 2 times the patch depth, or  $2D_r$ . Defining the wave slope,  $\chi$ , according to  $\chi = H_s/\lambda$ , the fractional breaking scale is therefore equal to  $4\chi$ . This takes values of 0.1–0.2 over the set of data periods (see Table 1 of Part I), within the range of values of 0.1–0.4 following from the acoustic observations of Ding and Farmer (1994; see Graham and Hall 1997). It may similarly be expected that length  $(\nu \Delta t)^{1/2}$  constitute some (much smaller) fraction,  $k_\lambda$ , of  $\lambda$ . Thus,  $Q_L = k_\lambda \chi$ , where  $k_\lambda \doteq 2/k_\lambda$ . It should be noted that the measurements of bubble populations, made on calibrating the images, support the generation of bubble clouds by a breaking of waves characteristically intermediate in scale, shorter than the dominant waves but yet to equilibrate at a limiting height (see Part I).

Observations of deep-water breaking waves in the laboratory show the convective velocity of the largest eddies to scale with the phase speed, as a factor of 0.01–0.02 on cessation of breaking, with little dependence on wave energy apparent (Rapp and Melville 1990). It follows from (2) that  $Q_v$  and  $\Delta t$  are also independent of wave energy. A value for the ratio of cloud-generating to dominant wavelengths of 0.4 may realistically be adopted (see the discussion of Part I). The identification,  $Q_v(\nu/\Delta t)^{1/2} = \kappa_v(g\lambda)^{1/2}$ , may thus be made from (2) (with  $\tau = 0$ ), where  $\kappa_v = 4 \times 10^{-3}$ . Rearranging and substituting for  $\Delta t$  leads to the relation,  $Q_v = \kappa_v \kappa_\lambda (g\lambda^3)^{1/2}/\nu$ .

For the sonar measurements, values of  $f_i$  are positively correlated with  $\chi$  (but not with wind speed or ratio of wind speed to phase speed). Consequently, from Eq. (A3) in appendix A, it is supposed  $\chi$  determines  $N$ , the frequency of bubble cloud generation per unit sea surface area, as well as  $Q_L$ . For the *dimensions* of  $N$  appeal is made to the equilibrium subrange of the wave spectrum (though the waves breaking and generating clouds are characteristically somewhat longer than these waves). The dimensions of subrange parameters depend only on  $g$  and wavelength  $\lambda$ . Instances of breaking over

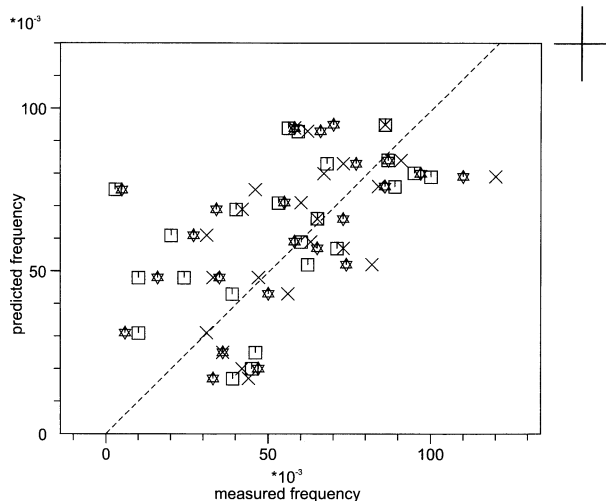


FIG. 2. Plot of predicted mean frequencies of occurrence of bubble clouds at a fixed point vs values measured using sonar, frequencies as normalized by that of the dominant waves. Values obtained at the depth where measured frequencies are highest. Clouds are deemed present in the sonar beam records from sustained episodes in which the signal exceeds its median value. Crosses show measurements obtained at an acoustic frequency of 86 kHz, squares at 250 kHz, and starts at 500 kHz. The dashed line shows equivalence, and the top-right-hand cross shows the standard error of the data.

a range of wavelengths,  $d\Lambda$ , may thus be expected to occur at a rate per unit area scaling with  $(g/\Lambda^7)^{1/2}d\Lambda$ . The identification  $N = k_N\chi^M(g/\lambda^5)^{1/2}$  is therefore made, where  $k_N$  is a (dimensionless) constant to be determined and power  $M$  is also to be specified.

Least squares fits of  $f_i$  to values predicted according to (A3) may be derived as a function of  $\lambda$ ,  $\chi$ , and current speed  $u$ . Figure 2 shows a fit as holds in the case  $M = 2$ . As  $N$  may be assumed to increase nonlinearly with  $\chi$  and fits at higher values of  $M$  are not significantly tighter, this is the value adopted. Corresponding values of coefficients are then  $k_L = 3 \times 10^4$ ,  $k_N = 50$ . It follows that  $k_\lambda = 7 \times 10^{-5}$ .

Values of  $\Delta t$  computed from  $k_\lambda$  and normalized by the dominant wave period  $T$  are of median 0.9 over the set of data periods. Time  $\Delta t$  is thus broadly comparable to the duration of wave breaking,  $t_b$ , as to be expected if the model holds true. The turbulent patch generated during breaking initially deepens at a speed equal, from (1), to  $Q_L(\nu/\Delta t)^{1/2}/2$ . Values of this normalized by the orbital velocity associated with the dominant waves, estimated as  $\pi H_s/T$ , are of median 0.4 over the set of data periods. Laboratory observations of deep water breaking show deepening speeds and orbital velocities initially to be comparable (see the review section of Part I). The discrepancy may further reflect a breaking of waves characteristically shorter than the dominant waves.

A value of  $k_N = 50$  implies frequencies of bubble-cloud generation per unit sea surface area an order of magnitude smaller than the areal frequencies of breaking

with air entrainment measured by Ding and Farmer (1994) and Phillips et al. (2001). This is reasonable, because it is to be expected that most breaking events with air entrainment involve shorter waves than those giving rise to persistent bubble clouds (see section 1).

The frequency with which cloud generation occurs at a point at the surface,  $f_b$ , is the rate at which generation events are initiated within a distance,  $Q_L(\nu\Delta t)^{1/2}$ , from the point so that  $f_b = \pi Q_L^2\nu\Delta tN$ . With parameters as expressed above, it follows that  $f_b$  in deep water is a factor of  $1.6 \times 10^3\chi^4$  times the dominant wave frequency. A dependence on wave slope is also identified by Banner et al. (2000) as to the square once a critical threshold is removed. The dependence conflicts with that identified by Thorpe (1993), comprising a spot frequency of breaking a factor of  $4.0 \times 10^{-3}\gamma^{-3}$  times the dominant wave frequency, where  $\gamma$  is the wave age, or ratio of phase speed of the dominant waves to (10 m) wind speed. The disparity suggests that, even at sites where fetch and water depth limit wave development, the frequency of breaking depends incompletely on the degree of development, at least in so far as this is parameterized through a wave age.

Over the set of data periods, values of Thorpe's factor are of median 5 times the median of the factor deduced here. The disparity is less than that described above between areal frequencies. This is to be expected given that the events in which clouds are generated, though infrequent, involve entrainment over a relatively large area of sea surface, and so may commence farther from a point and still be observed there.

The wave breaking that gives rise to persistent bubble clouds contributes to the active whitecap fraction. The contributory term may be estimated as  $f_b t_b$ . Taking  $t_b$  as a factor, 0.3, of  $T$ —within the range of factors 0.2–0.5 following from the measurements of Ding and Farmer (1994)—it follows that  $f_b t_b = 500\chi^4$ . The range of values of this computed over the set of data periods is the same as that of measurements of active whitecap fraction made by video at the site by Kraan et al. (1996). Monahan and O'Muircheartaigh (1980) and Andreas and Monahan (2000) parameterize whitecap fraction as scaling simply with wind speed, to a power of between 3 and 4, the active fraction taking a value of 0.05% at a (10 m) wind speed of  $10 \text{ m s}^{-1}$ . Values of  $f_b t_b$  computed over the set of data periods are of median about twice that of values obtained using the expression of Andreas and Monahan. The infrequent breaking events in which clouds are generated may thus contribute more to whitecap fractions than to spot breaking frequencies, as might be expected given that the entrainment takes place over relatively long durations as well as large length scales.

*b. Bubble population*

The bubble-size distribution on cessation of breaking must fall off sharply for radii in excess of a value,  $a_m(0)$ ,

as may be predicted according to (5). Given the dependence on conditions of  $Q_v/\Delta t^{1/2}$  identifiable from section 3a, it follows that  $a_m(0)$  scales with  $(v^2\lambda^3/g)^{1/6}$ , with a coefficient of  $k_v/Q_a = 7 \times 10^{-3}$ . Corresponding values range through 200–400  $\mu\text{m}$  over the set of data periods (see Table 1 in Part I). Few bubbles in excess of 500- $\mu\text{m}$  radius would be anticipated to persist after breaking, these being prone to instability as they rise through their surroundings (see section 2). That  $a_m(0)$  is significantly less than 500  $\mu\text{m}$  supports the original hypothesis that losses to the surface rather than stabilization by surface tension limits bubble size from the cessation of breaking onward.

The sonar images of bubble clouds have been calibrated so as to yield bubble concentrations (see the analysis of Part I). Statistics of two bulk bubble parameters—the total bubble surface area under unit sea surface,  $A_b$ , and the upward displacement of the sea surface by bubbles,  $z_b$ —are obtained for each data period. Examination of medians shows  $A_b$  and  $z_b$  to increase as wind speed to the powers  $7 \pm 1$  and  $8 \pm 1$ , respectively, as shown in Fig. 16 in Part I, and as described further therein (note that significant dependences on  $H_s$  and  $\lambda$  are not observed). Mean values can be measured accurately in a (10 m) wind,  $W_{10}$ , of around 6  $\text{m s}^{-1}$  or less. The ratio of mean to median in such cases can then be used to assign an appropriate value to the bubble-size distribution power  $q$  (see section 2). The ratio is predicted to increase with  $q$  according to (B9) and (B10) in appendix B.

A value of  $q = 0.25$  results. This, together with a reference value of  $B = 1 \times 10^{-3}$ , the median of values of  $B$  computed for the data periods contributing to Fig. 16, have been used to generate fit B shown in each plot. That  $q < 1$  indicates the bubble size distribution reaches peak or near-peak values at radii significantly smaller than  $a_m(0)$  on cessation of breaking (see section 2). Whether this, in turn, evidences a peak radius of bubble generation smaller than  $a_m(0)$  is, perhaps, a moot point (see Garrett et al. 2000).

The mean bubble radius, summing over all depths and averaging over time,  $\xi\{a\}$ , is predicted to scale with  $a_m(0)$  according to (B3). This relation may be evaluated further on adopting a value of  $q = 0.25$  and with  $B$  and  $a_m(0)$  depending on conditions according to expressions given earlier in the section. It follows that  $\xi\{a\}$  scales with  $H_s$ , with an approximately constant coefficient of  $3 \times 10^{-5}$ . Values of  $\xi\{a\}$  obtained directly from the measurements (at 0.4-m depth) do not show a significant scaling with  $H_s$  (see Part I) but may be biased as they exclude strongly scattering bubble clouds (likely to be among the youngest and thus to contain more large bubbles). Ratios of  $\xi\{a\}/H_s$  are of median over the set of data periods equal to the predicted coefficient.

Values of the bulk bubble parameters on cessation of breaking,  $A_b(0)$  and  $z_b(0)$ , may be estimated. These parameters likely carry the strong dependences on wind speed observed in the statistics of  $A_b$  and  $z_b$  (see Part

I). Area  $A_b(0)$  may thus be taken to increase as wind speed to the power 7. Instantaneous values of  $A_b$  at a reference wind speed of  $W_{10} = 10 \text{ m s}^{-1}$  are, from Part I, of median 0.24% of the overlying sea surface area. The median may be related to  $A_b(0)$  through the theory of appendix B. On adopting a value  $q = 0.25$  and a reference value  $B = 1 \times 10^{-3}$ , as above, it follows from (B6) that  $A_b(0)$  at  $W_{10} = 10 \text{ m s}^{-1}$  is about a factor of 13 times the sea surface area above the bubbles.

Displacement  $z_b(0)$  is analogously taken to increase as wind speed to the power 8. From (B11) (and with  $q = 0.25$ ),  $z_b(0)/a_m(0) = 0.25A_b(0)$ . Thus, at a reference wind speed of  $W_{10} = 10 \text{ m s}^{-1}$  bubbles on cessation of breaking are estimated to displace the sea surface upward by a factor of 3 times  $a_m(0)$ .

The wind speed dependencies likely result from a breaking of waves characteristically too short for their energy to correlate with that of the spectral peak (see part I). From the laboratory measurements of Lamarre and Melville (1994),  $z_b(0)$ , expressed as a fraction of the height of the breaking waves, may be calculated to be a factor of 0.7 times the square of their slope (see the review section of Part I). Values of  $z_b(0)/H_s$  computed over the set of data periods considered here are of median a factor of 0.5 times the square of the dominant wave slope. Thus, if the waves characteristically breaking are of height equal to about  $0.5H_s$  and, as supposed in section 3a, are of wavelength  $0.4\lambda$ , laboratory and field measurements may broadly be reconciled.

### c. Bubble-mediated trace-gas exchange

The case of carbon dioxide is considered. The solubility coefficient  $\beta$  in (7) is then equal to 0.8. As bubbles are found in section 3b, to be less than 500  $\mu\text{m}$  in radius, a constant single-bubble transfer velocity,  $\kappa_b$ , of 45  $\text{cm h}^{-1}$  is taken as appropriate (see section 2). The time constant of transfer in the bubbles,  $\tau_c$ , is therefore less than a wave period (see section 2), and the transfer will effectively cease soon after breaking.

A transfer velocity as integrated over all bubbles and bubble ages,  $K_b$ , may be calculated, as shown in appendix C. It scales with both  $\kappa_b$  and  $A_b(0)$  (the latter as defined and estimated in section 3b), as can be seen from (C2). On setting  $q = 0.25$  and evaluating dimensionless variables  $B$  and  $C$  according to conditions, values of the scaling coefficient may be computed, and are of median,  $3 \times 10^{-4}$ , over the set of data periods (see Table 1 of part I). In a wind of  $10 \text{ m s}^{-1}$ , it follows that the best prediction of  $K_b$  is about 0.4% of  $\kappa_b$ , or 0.2  $\text{cm h}^{-1}$ . The subsurface transfer of carbon dioxide following breaking does not, therefore, contribute significantly to the total time-averaged transfer. Woolf (1993) estimates—without the data on breaking frequencies and bubble concentrations obtained here—that the subsurface transfer including that accomplished during breaking takes place at 8.5  $\text{cm h}^{-1}$  at comparable wind speeds.

#### 4. Concluding remarks

Aeration of the sea due to a breaking of waves generated by wind has been parameterized using an analytic model, and parameter values have been established from measurements of bubble populations obtained in a recent experiment. In the model, waves sporadically break in discrete events in which persistent bubble clouds are generated; these then grow and release entrained air back to the surface at rates dependent on the largest of the eddies generated. The measurements were acquired acoustically at a coastal site not subject to oceanic swell.

Bubble clouds are generated at an estimated rate,  $50\chi^2(g/\lambda^5)^{1/2}$ , per unit sea surface area, where  $\chi$  is the dominant wave slope, or ratio of significant wave height  $H_s$  to energetically dominant wavelength  $\lambda$ , and  $g$  is the acceleration due to gravity. Entrainment distributes bubbles over a volume of equivalent hemispherical radius,  $L = 2H_s$ . Cloud generation contributes a term,  $500\chi^4$ , to the active whitecap fraction. The fractional growth rate ascribed to  $L$  at the cessation of breaking is equal to  $10^8\nu/\lambda^2$ , where  $\nu$  is the kinematic viscosity of seawater.

The entrainment of air during breaking involves a complex turbulent two-phase flow in which surface tension and water chemistry mediate (Garrett et al. 2000; Orris and Nicholas 2000; Wu 2000; Monahan 2001; Deane and Stokes 2002), and about which little can be said here. It is, however, argued that the largest bubbles held stable by surface tension as they rise persist only for a time comparable to the duration of breaking. The bubble size distribution on cessation of breaking falls off rapidly for bubbles in excess of a smaller size, radius  $a_m = 7 \times 10^{-3}(\nu^2\lambda^3/g)^{1/6}$ , because the turbulence is insufficient to sustain larger bubbles subsurface by opposing their buoyancy. A further calculation shows the surface area of bubbles then entrained per unit area of sea surface,  $A_b$ , to be related to their upward displacement of the surface, or volume of air entrained per unit sea surface area  $z_b$ , according to  $z_b/a_m = 0.25A_b$ . Measurements indicate that  $A_b$  increases with wind speed as to a power  $7 \pm 1$ , with its value at a (10 m) wind speed of  $W_{10} = 10 \text{ m s}^{-1}$  estimated to be 13 at the site.

Although  $A_b$  may be calculated to exceed unity in winds in excess of  $W_{10} = 7 \text{ m s}^{-1}$ , the total bubble surface area and rate of gas exchange across bubble walls fall rapidly after breaking. Calculations of the air-sea transfer of carbon dioxide thus need not take into account the transfer accomplished within bubble clouds from the cessation of breaking onward, a finding in accord with Woolf (1993).

*Acknowledgments.* European partners of the ASGA-MAGE experiment were funded through EC Grant MAS3-CT95-0044. I am grateful to Prof. S. Thorpe, Dr. D. Woolf, and two anonymous referees for their helpful comments on the manuscript.

#### APPENDIX A

##### Parameterization of the Bubble-Cloud Distribution

Sonar images of bubble clouds have been obtained and are used to profile the frequency with which clouds are observed in an Eulerian reference frame (see Part I). It is now sought to predict observation frequencies from a model (section 2) for comparison with measurement.

A technique applied to the images to identify clouds objectively captures the large-scale, strongly scattering coherent structure present (see the analysis of Part I). Shapes are derived from the images from points where the signal exceeds a threshold value, that associated with a prescribed percentile of the signal histogram at each depth (each histogram thus as built up over the data period). The shapes may be interpreted as resulting from the youngest clouds, the volume of air they hold declining as they age and their bubbles reach the surface and burst (see section 2).

An expression is thus sought for the mean frequency  $f_i$  of episodes in which clouds of some age  $\tau_i$  or younger occur at a fixed observation point. Bubbles are taken to be distributed throughout the turbulent patch in which they reside in some depth-dependent manner. The reference observation depth is chosen to be that to which clouds extend when first generated,  $D_g$ . This depth may be derived from the images (see the results, section 3). Thus,  $D_g = L(\tau = 0)$  and, so, from (1)  $D_g = Q_L(\nu\Delta t)^{1/2}$ . The histogram percentile referred to above in the analysis of the images may be identified as the probability of a cloud of age  $\tau_i$  or younger occurring at the observation point,  $P_i$ .

An expression for  $P_i$  may be derived in the same manner as that adopted in section 2 [the probability therein denoted  $P(\tau \leq \tau_i)$ ], on extending the treatment so that it applies at a depth  $D_g$ . It can be seen that a cloud of age  $\tau$  at this depth is of horizontal radius  $r$  given by  $r = Q_L(\nu\tau)^{1/2}$ . As  $r = 0$  when  $\tau = 0$ , an expression for  $P_i$  follows on setting  $\Delta t = 0$  in (11). Thus,  $P_i = 1 - \exp[-\pi\nu(Q_L\tau_i)^2N/2]$ . This may be rearranged to yield the following identity:

$$\pi Q_L^2 \nu \tau_i N = [2\pi Q_L^2 \nu N \log_e(1 - P_i)^{-1}]^{1/2}. \quad (\text{A1})$$

A fresh episode in which young clouds are distinguished at the observation point may begin if the pre-existing cloud is older than  $\tau_i$ . The probability that this holds is  $1 - P_i$ . Frequency  $f_i$ , it follows, is given by  $f_i = AN(1 - P_i)$ , where  $A$  is the horizontal area in which clouds must be engendered to be of age  $\tau_i$  or younger when arriving at the observation point. If there is no current,  $A$  takes a value,  $A_0$ , given by  $A_0 = \pi Q_L^2 \nu \tau_i$ , so that  $f_i = \pi Q_L^2 \nu \tau_i N(1 - P_i)$ . On substituting (A1) into this, it follows that

$$f_i = [2\pi Q_L^2 \nu N \log_e(1 - P_i)^{-1}]^{1/2}(1 - P_i). \quad (\text{A2})$$

In the general case, in the presence of a mean flow  $u$ ,

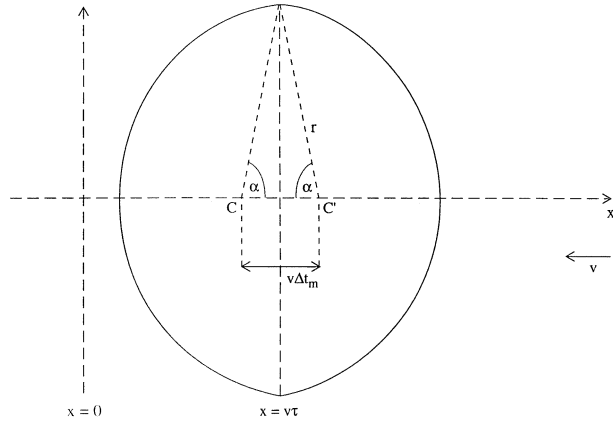


FIG. A1. Plan view showing the locus clouds must originate on to be of age  $\tau$  when identified by the fixed observer at a depth  $D_s$  at the origin. The locus comprises arcs of identical circles centered at C and C', their common chord lying along  $x = v\tau$ , where  $v$  is the mean flow. Other symbols are as in the text.

$$f_t = S[2\pi Q_L^2 \nu N \log_e(1 - P_t)^{-1}]^{1/2}(1 - P_t), \quad (\text{A3})$$

where  $S \doteq A/A_0$ .

To detect young clouds an observer will, in practice, require a short appraisal time  $\Delta t_m$  (10 s in the analysis of the sonar images to smooth out inhomogeneities within the clouds and noise). Time  $\tau_t$  and  $P_t$  may be presumed high enough that  $\Delta t_m/\tau_t \ll 1$  (this can be validated from the results of section 3). In the presence of a strong current, however, some clouds may be advected through the beam in a time comparable to  $\Delta t_m$ , and thus not be observed. The effect may conveniently be allowed for by requiring that, for a young cloud to be distinguished at the observation point, it must originate along the locus shown in Fig. A1.

Function  $S$  changes smoothly with  $v$  over at most three regimes, as described below. It has a maximum at the following value:

$$v = Q_L[(\nu/\Delta t_m)(\tau_t/\Delta t_m - 3/4)]^{1/2}, \quad (\text{A4})$$

if  $\Delta t_m/\tau_t \leq 4/7$ . For a current of speed,  $v = 2Q_L(\nu\tau_t)^{1/2}/\Delta t_m$  or more, a cloud of age  $\tau_t$  or younger cannot be detected, and  $S$  is zero.

The derivation is eased by introducing two time scales,  $\tau_c \doteq [\nu\Delta t_m/(2Q_L)]^2/\nu$  and  $\tau_b \doteq \nu[Q_L/(2v)]^2$ .

a.  $v \leq Q_L(\nu/\tau_t)^{1/2}/2$

Radius  $r$  grows at a rate no less than the speed of the current. The locus of origin of clouds of age  $\tau_t$  then encloses that of all younger clouds. Thus,  $A = Q_L^2 \nu \tau_t (2\alpha_t - \sin 2\alpha_t)$ , where  $\alpha_t \doteq \alpha(\tau_t)$  and  $\alpha$ , as shown in Fig. A1, satisfies  $\cos \alpha = v\Delta t_m/(2r) = (\tau_c/\tau)^{1/2}$ . Consequently,

$$S = (2\alpha_t - \sin 2\alpha_t)/\pi. \quad (\text{A5})$$

If  $\tau_t > \Delta t_m/4$ , clouds older than  $\tau_b$  may be identified, associated with a growth rate of  $r$  lower than the current

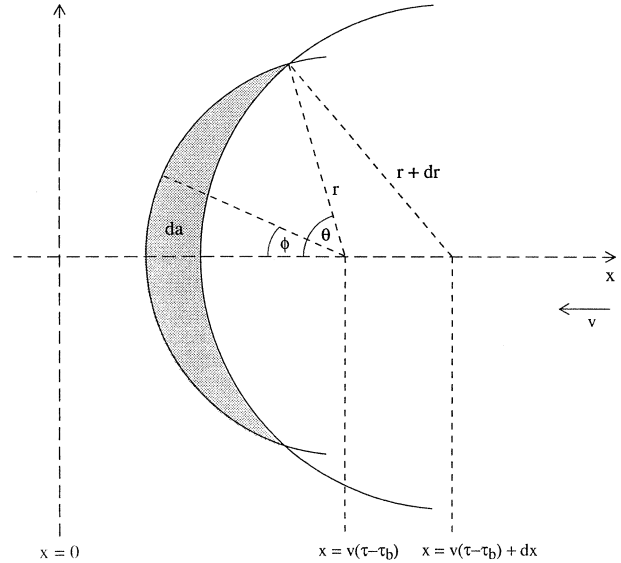


FIG. A2. Plan view in the same frame as in Fig. A1 showing the elemental area,  $da$ , between loci that clouds must originate on, if  $\tau \geq \tau_b$ , so as to be of ages  $\tau$  and  $\tau + d\tau$  on reaching the observer. It can be seen that  $\cos \theta = dr/dx$ . The portion of  $da$  within an angle  $\phi$  of the  $x$  axis is given by  $da_\phi = 2r(\sin \phi dx - \phi dr)$  so that  $da = da_\phi(\theta) = 2(\tan \theta - \theta)rdr$ .

speed, and two further regimes must be considered. Loci of origin no longer lie wholly within that of the oldest clouds, as shown in Fig. A2. As  $dx = v d\tau$ , so  $\cos \theta = (dr/d\tau)/v$ , giving  $\cos \theta = 2v\tau_b/r$  or, equivalently,  $\cos \theta = (\tau_b/\tau)^{1/2}$ .

b.  $Q_L(\nu/\tau_t)^{1/2}/2 \leq v \leq Q_L(\nu/\Delta t_m)^{1/2}$

The relation  $\theta \leq \alpha$  holds. The elemental area  $dA$  associated with clouds aged between  $\tau$  and  $\tau + d\tau$  is equal to the area  $da$  as shown in Fig. A2. The expression for  $dA$  may be recast, given that  $rdr = (2v\tau_b)^2(\sin \theta/\cos^3 \theta)d\theta$ , as

$$dA = (2v\tau_b)^2 \tan \theta (\tan^2 \theta + 1)(\tan \theta - \theta)d\theta. \quad (\text{A6})$$

Area  $A$  is then obtained by integrating this [noting that  $\theta(\tau_b) = 0$ ] and adding on the area identified in section a above. The following expression for  $S$  results:

$$S = [2\alpha_t - \sin 2\alpha_t + (1 - \sin^2 \theta_t/3) \tan \theta_t - \theta_t]/\pi, \quad (\text{A7})$$

where  $\theta_t \doteq \theta(\tau_t)$ .

c.  $v \geq Q_L(\nu/\Delta t_m)^{1/2}$

The relation  $\theta \geq \alpha$  holds. Setting  $\phi = \alpha$  (see Fig. A2),  $dA$  is the corresponding portion of  $da$ ,  $dA = 2r(\sin \alpha dx - \alpha dr)$ . Given that  $\cos \alpha = (dr/dx)(\tau_c/\tau_b)^{1/2}$  it can be seen that  $dA = 2[(\tau_c/\tau_b)^{1/2} \tan \alpha - \alpha]rdr$ . Substituting in a further relation,  $rdr = (v\Delta t_m/2)^2(\sin \alpha/\cos^3 \alpha)d\alpha$ , it follows that

$$dA = 2(\nu\Delta t_m/2)^2 \tan\alpha(\tan^2\alpha + 1) \\ \times [(\tau_c/\tau_b)^{1/2} \tan\alpha - \alpha] d\alpha. \quad (\text{A8})$$

In the same manner as in section b above,  $A$  is then obtained by integrating this [noting that  $\alpha(\tau_c) = 0$ ] and adding on the area identified in section a above so that

$$S = \langle \alpha_i + \{[1 + (2/3)(\tau_c/\tau_b)^{1/2}] \sin^2\alpha_i - 1\} \tan\alpha_i \rangle / \pi. \quad (\text{A9})$$

## APPENDIX B

### Parameterization of Bubble Populations

Bubble populations have been parameterized and measured (see Part I). It is now sought to predict some of these parameters using a model (section 2), for comparison with measurement.

In the model, the bubble population residing beneath the surface was generated in a previous breaking wave. Bubbles are taken as distributed in some depth-dependent manner throughout the turbulent patch simultaneously engendered. From (6) the mean bubble radius in a patch of age  $\tau$  is given by  $\int aG(a, \tau) da = q_1 a_m$ , where  $q_1 \doteq (q + 1)/(q + 2)$ . Substituting (4) into this it follows that  $\int aG(a, \tau) da = q_1 a_m(0)(1 + \tau_*)^{-1/2}$ . The unconditional, age-integrated, mean is thus given by

$$\xi\{a\} = q_1 a_m(0) \int_0^\infty (1 + \tau_*)^{1/2} p(\tau_*) d\tau_*, \quad (\text{B1})$$

where  $p(\tau_*)$  is given by (12) so that

$$\xi\{a\}/a_m(0) = q_1 B^{1/4} \exp(B)\Gamma(3/4, B), \quad (\text{B2})$$

where  $\Gamma$  is the incomplete Gamma function. Over the measurement set,  $B < 0.005$ , so (B2) may be approximated to within 2% as

$$\xi\{a\}/a_m(0) \approx 1.23q_1 B^{1/4}. \quad (\text{B3})$$

The total surface area of bubbles in a patch is equal to  $4\pi N_b \int a^2 G(a, 0) da$ , where  $N_b$  is the number of bubbles present below the surface on cessation of breaking, and the integration is performed over bubbles of up to radius  $a_m(\tau)$ . It can be seen that, on substitution of (6), this is equal to  $4\pi q_2 N_b [a_m/a_m(0)]^{q+3} a_m^2(0)$ , where  $q_2 \doteq (q + 1)/(q + 3)$ . On substitution of (4) this expression is, in turn, equal to  $4\pi q_2 N_b a_m^2(0)(1 + \tau_*)^{-(q+3)/2}$ . As the patch is of radius equal to  $L$ , as given by (1), the total bubble area, expressed as a fraction of the sea surface, is given by  $A_b = A_b(0)(1 + \tau_*)^{-(q+5)/2}$ , where

$$A_b(0) = 4q_2 N_b [a_m(0)/Q_L]^2 / (\nu\Delta t). \quad (\text{B4})$$

Area  $A_b$  thus varies with age such that it is of median value,  $\mu\{A_b\}$ , at the median value of  $\tau_*$ , which from (11) is given by

$$\mu\{\tau_*\} = [1 + (\log_e 2)/B]^{1/2} - 1. \quad (\text{B5})$$

Thus,

$$\mu\{A_b\} = A_b(0)[1 + (\log_e 2)/B]^{-(q+5)/4}. \quad (\text{B6})$$

The mean value of  $A_b$  is given by

$$\xi\{A_b\} = A_b(0) \int_0^\infty (1 + \tau_*)^{-(q+5)/2} p(\tau_*) d\tau_*. \quad (\text{B7})$$

Given that  $B < 1$  and anticipating that a value,  $q \leq 1$ , is appropriate (as is shown in the results, section 3), the following relation holds:

$$\xi\{A_b\} = [4A_b(0)/(q + 1)] \\ \times B\{1 - B^{(q+1)/4}\Gamma[(3 - q)/4, B]\}. \quad (\text{B8})$$

Thus,

$$\xi\{A_b\}/\mu\{A_b\} = [4/(q + 1)](\log_e 2)^{(q+5)/4} \\ \times \{B^{-(q+1)/4} - \Gamma[(3 - q)/4, B]\}. \quad (\text{B9})$$

Expressions may be derived in a similar manner for the upward displacement of the sea surface by bubbles,  $z_b$ , or the total bubble volume under unit sea surface area. The predicted relation between mean and median is the following,

$$\xi\{z_b\}/\mu\{z_b\} = [4/(q + 2)](\log_e 2)^{(q+6)/4} \\ \times \{B^{-(q+2)/4} - \Gamma[(2 - q)/4, B]\}, \quad (\text{B10})$$

and  $A_b(0)$  and  $z_b(0)$  are related as follows:

$$z_b(0)/a_m(0) = [(q + 3)/(q + 4)]A_b(0)/3. \quad (\text{B11})$$

## APPENDIX C

### Parameterization of Bubble-Mediated Trace-Gas Exchange

The mass flux between a single bubble and its surroundings is described in section 2. It is now sought to predict the bubble-integrated gas flux using a model of bubble formation and evolution developed therein.

In the model, the bubble population residing beneath the surface was generated in a previous breaking wave. Bubbles are taken as distributed in some depth-dependent manner throughout the turbulent patch simultaneously engendered. The patch is of radius equal to  $L$  as given by (1). The total rate of mass transfer under unit sea surface area for a cloud of age  $\tau$  is given by

$$- \{N_b / [\pi Q_L^2 \nu(\Delta t + \tau)]\} \int_0^{a_m(\tau)} \dot{m}_b(a, \tau) G(a, 0) da,$$

where  $N_b$  is as in appendix B, and  $G$  and  $\dot{m}_b$  are given by (6) and (7), respectively. The total mass flux from bubbles is thus of mean, age-integrated value,  $F_b$ , given by

$$F_b = - \left[ \frac{N_b}{(\pi Q_L^2 \nu \Delta t)} \right] \\ \times \int_0^\infty \int_0^{a_m(\tau_*)} \left[ \frac{\dot{m}_b(a, \tau_*)}{1 + \tau_*} \right] G(a, 0) p(\tau_*) da d\tau_*. \quad (\text{C1})$$

A transfer velocity  $K_b$  may be used to parameterize bubble-integrated gas transfer in the same way as such a velocity is used to parameterize gas transfer across the sea surface (see the introduction to part I). It is thus defined according to the relation,  $F_b = K_b(\beta C_a - C_w)$ , where  $\beta$ ,  $C_a$ , and  $C_w$  are as defined in section 2. On equating the two expressions for  $F_b$  above and substituting in (4), (6), (7), and (12) the following relation between single and total bubble transfer velocities results:

$$\frac{K_b}{\kappa_b} = 2(q + 3)A_b(0)B \times \int_0^\infty \int_{(1+\tau_w)^{1/2}}^\infty y^{-(q+4)} \exp\{-[B(2 + \tau_*) + Cy]\tau_*\} dy d\tau_*, \quad (C2)$$

where  $y \doteq a_m(0)/a$ ,  $C \doteq 3\beta\kappa_b\Delta t/a_m(0)$ , and  $A_b(0)$  is as for appendix B.

#### REFERENCES

- Andreas, E. L., and E. C. Monahan, 2000: The role of whitecap bubbles in air–sea heat and moisture exchange. *J. Phys. Oceanogr.*, **30**, 433–442.
- Banner, M. L., A. V. Babanin, and I. R. Young, 2000: Breaking probability for dominant waves on the sea surface. *J. Phys. Oceanogr.*, **30**, 3145–3160.
- Batchelor, G. K., 1953: *The Theory of Homogeneous Turbulence*. Cambridge University Press, 197 pp.
- Belcher, S. E., and J. C. Vassilicos, 1997: Breaking waves and the equilibrium range of wind-wave spectra. *J. Fluid Mech.*, **342**, 377–401.
- Clift, R., J. R. Grace, and M. E. Weber, 1978: *Bubbles, Drops, and Particles*. Academic Press, 380 pp.
- Csanady, G. T., 1994: Vortex pair model of Langmuir circulation. *J. Mar. Res.*, **52**, 559–581.
- Dahl, P. H., and A. T. Jessup, 1995: On bubble clouds produced by breaking waves: An event analysis of ocean acoustic measurements. *J. Geophys. Res.*, **100**, 5007–5020.
- Deane, G. B., and M. D. Stokes, 2002: Scale dependence of bubble creation mechanisms in breaking waves. *Nature*, **418**, 839–844.
- Ding, L., and D. M. Farmer, 1994: Observations of breaking surface wave statistics. *J. Phys. Oceanogr.*, **24**, 1368–1387.
- Donelan, M., M. S. Longuet-Higgins, and J. S. Turner, 1972: Periodicity in whitecaps. *Nature*, **239**, 449–451.
- Garrett, C., M. Li, and D. Farmer, 2000: The connection between bubble size spectra and energy dissipation rates in the upper ocean. *J. Phys. Oceanogr.*, **30**, 2163–2171.
- Gemmrich, J., and L. Hasse, 1992: Small-scale surface streaming under natural conditions as effective in air–sea gas exchange. *Tellus*, **44B**, 150–159.
- Graham, A., D. K. Woolf, and A. J. Hall, 2004: Aeration due to breaking waves. Part I: Bubble populations. *J. Phys. Oceanogr.*, **34**, 989–1007.
- , and A. J. Hall, 1997: The horizontal distribution of bubbles in a shallow sea. *Cont. Shelf Res.*, **17**, 1051–1082.
- Harper, J. F., 1972: The motion of bubbles and drops through liquids. *Adv. Appl. Mech.*, **12**, 59–129.
- Hunt, J. C. R., and J. M. R. Graham, 1978: Free stream turbulence near plane boundaries. *J. Fluid Mech.*, **84**, 209–235.
- Kerman, B. R., and L. Bernier, 1994: Multifractal representation of breaking waves on the ocean surface. *J. Geophys. Res.*, **99**, 16 179–16 196.
- Kraan, C., W. A. Oost, and P. A. E. M. Janssen, 1996: Wave energy dissipation by whitecaps. *J. Atmos. Oceanic Technol.*, **13**, 262–267.
- Lamarre, E., and W. K. Melville, 1994: Void-fraction measurements and sound-speed fields in bubble plumes generated by breaking waves. *J. Acoust. Soc. Amer.*, **95**, 1317–1328.
- Melville, W. K., 1996: The role of surface-wave breaking in air–sea interaction. *Annu. Rev. Fluid Mech.*, **28**, 279–321.
- Monahan, E. C., 2001: Comments on “Bubbles Produced by Breaking Waves in Fresh and Salt Water.” *J. Phys. Oceanogr.*, **31**, 1931–1932.
- , and I. G. O’Muircheartaigh, 1980: Optimal power-law description of oceanic whitecap coverage dependence on wind speed. *J. Phys. Oceanogr.*, **10**, 2094–2099.
- Nepf, H. M., E. A. Cowen, S. J. Kimmel, and S. G. Monismith, 1995: Longitudinal vortices beneath breaking waves. *J. Geophys. Res.*, **100**, 16 211–16 221.
- Orris, M. J., and M. Nicholas, 2000: Collective oscillations of fresh and salt water bubble plumes. *J. Acoust. Soc. Amer.*, **107**, 771–787.
- Osborn, T., D. M. Farmer, S. Vagle, S. A. Thorpe, and M. Cure, 1992: Measurements of bubble plumes and turbulence from a submarine. *Atmos.–Ocean*, **30**, 419–440.
- Phillips, O. M., F. L. Posner, and J. P. Hansen, 2001: High range resolution radar measurements of the speed distribution of breaking events in wind-generated ocean waves: Surface impulse and wave energy dissipation rates. *J. Phys. Oceanogr.*, **31**, 450–460.
- Rapp, R. J., and W. K. Melville, 1990: Laboratory models of deep-water breaking waves. *Philos. Trans. Roy. Soc. London*, **A331**, 735–800.
- Smith, M. J., E. M. Poulter, and J. A. McGregor, 1996: Doppler radar measurements of wave groups and breaking waves. *J. Geophys. Res.*, **101**, 14 269–14 282.
- Thorpe, S. A., 1982: On the clouds of bubbles formed by breaking wind-waves in deep water, and their role in air–sea gas transfer. *Philos. Trans. Roy. Soc. London*, **A304**, 155–210.
- , 1986: Measurements with an automatically recording inverted echo sounder; ARIES and the bubble clouds. *J. Phys. Oceanogr.*, **16**, 1462–1478.
- , 1993: Energy loss by breaking waves. *J. Phys. Oceanogr.*, **23**, 2498–2502.
- , 1995: Dynamical processes of transfer at the sea surface. *Progress in Oceanography*, Vol. 35, Pergamon, 315–352.
- , and A. J. Hall, 1983: The characteristics of breaking waves, bubble clouds, and near-surface currents observed using side-scan sonar. *Cont. Shelf Res.*, **1**, 353–384.
- , A. Nimmo Smith, A. M. Thurnherr, and N. J. Walters, 1999: Patterns in foam. *Weather*, **54**, 327–334.
- Woolf, D. K., 1993: Bubbles and the air–sea transfer velocity of gases. *Atmos.–Ocean*, **31**, 517–540.
- , and S. A. Thorpe, 1991: Bubbles and the air–sea exchange of gases in near-saturation conditions. *J. Mar. Res.*, **49**, 435–466.
- Wu, J., 2000: Bubbles produced by breaking waves in fresh and salt waters. *J. Phys. Oceanogr.*, **30**, 1809–1813.